The preparation of double-walled carbon nanotube/Cu composites by spark plasma sintering, and their hardness and friction properties

Ch. Guiderdoni [a], *C. Estournès* [b], *A. Peigney* [a], *A. Weibel* [a], *V. Turq* [a], *Ch. Laurent* [a,*]

[a] *Université de Toulouse, Institut Carnot CIRIMAT, UMR CNRS-UPS-INP 5085, Université Paul-Sabatier, 118 route de Narbonne, 31062 Toulouse Cedex 9, France*

[b] *CNRS, Institut Carnot CIRIMAT, UMR CNRS-UPS-INP 5085, 118 route de Narbonne, 31062 Toulouse Cedex 9, France*

A B S T R A C T

Double-walled carbon nanotube (DWCNT)/copper composite powders were prepared by a rapid route involving freeze-drying without oxidative acidic treatment or ball-milling. The DWCNTs are not damaged and are homogeneously dispersed in the matrix. Dense specimens were prepared by spark plasma sintering. The Vickers microhardness is doubled, the wear against a steel or an alumina ball seems very low and the average friction coefficient is decreased by a factor of about 4 compared to pure copper. The best results are obtained for a carbon loading (5 vol%) significantly lower than those reported when using multi-walled carbon nanotubes (10–20 vol%). Maximum Hertzian contact pressure data could indicate that the surface DWCNTs and bundles of them are deformed and broken, possibly resulting in the formation of a graphitized lubricating tribofilm in the contact.

. Introduction

The interest in using carbon nanotubes (CNTs) in metal–matrix composites is growing because of the unique mechanical and physical properties of the CNTs, which could make such materials promising for structural as well as functional applications. A recent review in this field [1] indicates that only a few reports address the study of the tribological properties of composite coatings or bulk materials, although self-lubricating materials, obviating the need for liquid lubricants, are very promising for applications. The homogeneity of the CNT dispersion into the matrix, a good interfacial bonding and a high relative density have been identified as key points to achieve good results, i.e. a higher microhardness, lower friction and lower wear [2–12]. In particular, a research group has studied the tribological properties of CNT/Cu composites [2–4] containing multi-walled CNTs (MWCNTs) 10–40 nm in diameter. The composites preparation process included acidic treatment of the MWCNTs, electroless nickel-coating, ball-milling with a Cu powder, isostatically pressing, natural sintering and sometimes post-sintering cold-rolling and annealing. It is claimed that electroless nickel-coating improves the interfacial bonding strength with the Cu–matrix. Other researchers [6,7] prepared MWCNT/Cu composites by spark plasma sintering (SPS) of composite powders prepared by the so-called molecular-level mixing process, involving suspending MWCNTs (10–40 nm in diameter) in solvent by surface functionalization, mixing Cu salts with the MWCNT suspension, drying, calcination and reduction prior to their densification. CNT–Al composites [10] were prepared by SPS of powders prepared by mixing under ultrasonic agitation an Al powder with CNTs previously oxidized by refluxing in nitric acid. It is claimed that this route produces a good dispersion of the CNTs and an optimum interfacial bond. Acidic treatments, however desirable to functionalize the CNT outer walls, may lead to strong damage [13]. Likewise, ball-milling

* *Corresponding author.*
E-mail address: laurent@chimie.ups-tlse.fr (Ch. Laurent).

doi:10.1016/j.carbon.2011.06.063

may cut and damage the CNTs and it is also possible that CNT agglomeration during the drying of a liquid suspension will cause a poor dispersion. Therefore, the aims of this work are firstly to prepare CNT/Cu composite powders using a simple way involving the freeze-drying route, which was reported [14] to be efficient in preventing CNT segregation for MWCNT–Al_2O_3 composites, and secondly to densify them by SPS and investigate their microhardness and tribological properties. In the present study, double-walled CNTs (DWCNTs) are used. They differ from the MWCNTs used by other researchers in several aspects, namely length/diameter ratio, defect proportion, mechanical properties and tendency to gather into bundles. In addition, a given DWCNT weights much less than a MWCNT of the same length [15] and therefore much more DWCNTs will be present for a certain carbon weight loading, which can greatly modify the matrix microstructure and ultimately give better results for lower carbon loadings, as was evidenced for DWCNT–ceramic composites [16–18].

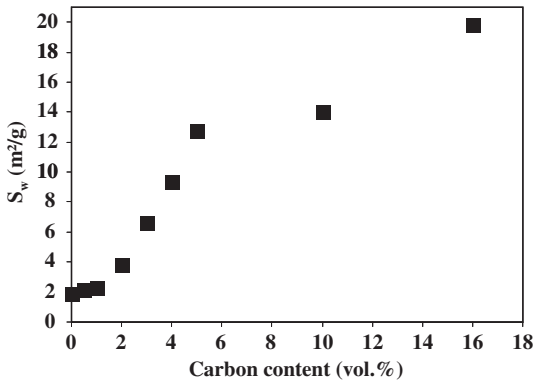

Fig. 1 – Specific surface area of the DWCNT/Cu powder versus the carbon content.

2. Experimental methods

2.1. *Powder synthesis*

A CuO powder was prepared by the oxalate precipitation/calcination route. The appropriate amounts of $Cu(NO_3)_2{\cdot}6H_2O$ and $(NH_4)_2C_2O_4{\cdot}2H_2O$ were dissolved in deionized water. The solution was rapidly poured into ethanol, where precipitation of CuC_2O_4 occurred immediately, and was kept under stirring for 1 h. The precipitate was filtered, washed with ethanol and dried overnight at 80 °C, producing a CuC_2O_4 powder. This powder was decomposed in air at 400 °C, producing a cupric oxide (CuO) powder. A Cu powder was prepared by reduction of CuO in H_2 at 400 °C. Heating and cooling rates were equal to 100 °C/h and a dwell was applied at 400 °C for 1 h. CNTs were synthesized by the catalytic chemical vapor deposition

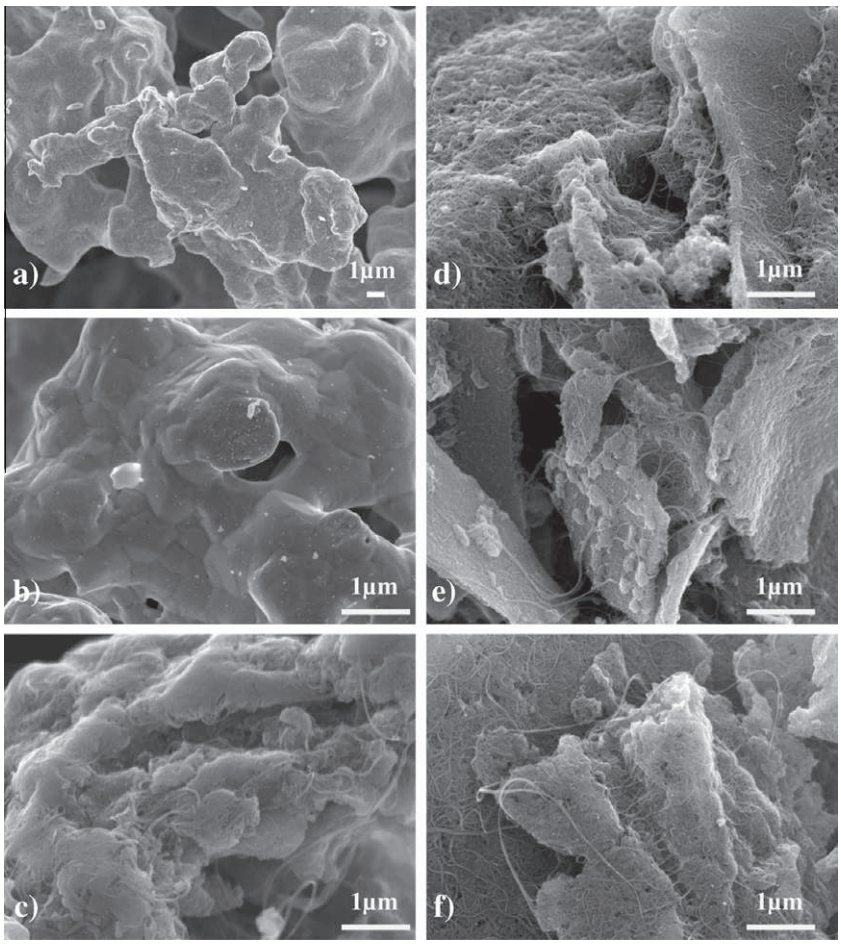

Fig. 2 – FESEM images of the Cu powder and composite powders P2 (b and c), P4 (d), P10 (e) and P16 (f).

(CCVD) route reported earlier [19]. The $Mg_{0.99}(Co_{0.75}Mo_{0.25})_{0.01}O$ catalytic material was submitted to a CCVD treatment (H_2–CH_4, 18 mol% CH_4, maximum temperature 1000 °C), producing a CNT–Co/Mo–MgO composite powder. This powder was soaked in a 37% HCl aqueous solution in order to dissolve MgO and most of the cobalt and molybdenum species, without damage to the CNTs [20]. The so-obtained suspension was washed with deionized water until neutrality, filtered and washed with ethanol. Finally, the sample was dried overnight at 80 °C in air. The carbon content (88.4 ± 0.2 wt% corresponding to ca. 97 mol%) was determined by flash combustion. The BET specific surface area is equal to 1000 ± 100 m^2/g. The CNTs in the sample are mostly DWCNTs (80%), SWCNTs (15%) and CNTs with three walls (5%), with the outer diameter in the range 1–3 nm and the inner diameter in the range 0.5–2.5 nm [19].

DWCNT/Cu composite powders with a carbon content C_n = 0.5, 1, 2, 3, 4, 5, 10 and 16 vol% were prepared by freeze-drying. They will be noted as P0.5, P1, ..., P16 hereafter. The appropriate weight amount of DWCNTs, calculated using the CNT density chart [15], was dispersed in deionized water with a sonotrode for a few seconds, after which the Cu powder was added. The ultrasonic agitation was maintained for 1 min. The vessel containing the DWCNT/Cu suspension was immersed in liquid N_2 for 2 min and freeze-dried (Christ Alpha 2-4 LD, Bioblock Scientific) at −40 °C for 48 h in a primary vacuum (12 Pa).

2.2. *Spark plasma sintering*

The pure Cu and DWCNT/Cu powders were consolidated by SPS (Dr. Sinter 2080, SPS Syntex Inc., Japan). They were loaded into a 20 mm inner diameter graphite die. A sheet of graphitic paper was placed between the punch and the powder as well as between the die and the powder for easy removal. This ensemble is known as the stack. The powders were sintered in vacuum (residual cell pressure < 10 Pa). A pulse pattern of 12 current pulses followed by two periods of zero current was used. A heating rate of 100 °C/min from room temperature to 700 °C, where a 6 min dwell was applied. The temperature was controlled using a thermocouple. A uniaxial charge (corresponding to 100 MPa) was gradually applied within the first minute of the dwell at 700 °C and maintained during the remaining 5 min. Natural cooling was applied down to room temperature. The uniaxial pressure was gradually released during cooling. The sintered specimens were in form of pellets 20 mm in diameter and about 2 mm thick. The pellets were polished down to 0.25 μm using diamond slurries. The sintered specimens will be noted as S0.5, S1, ..., S16 hereafter.

2.3. *Composition and microstructure characterization*

The specific surface area of the powders was measured by the BET method using N_2 adsorption at liquid-N_2 temperature (Micromeritics FlowSorb II 2300). The reproducibility of the results is ±3%. Detection and identification of crystalline phases was performed by X-ray diffraction (XRD) patterns analysis (Cu Kα radiation, Bruker D4 Endeavor) on powders and sintered pellets. The density of the pellets was calculated from their weight and dimensions. The relative densities were calculated using 1.8 for DWCNTs [15] and 8.92 for Cu. The powders and pellets were observed by field-emission-gun scanning electron microscopy (FESEM, JEOL JSM 6700F). For observation of the polished surfaces, the pellets were etched in HNO_3 (room temperature, 10 s). The roughness of the pellet surfaces was characterized with an interferential rugosimeter (NewView 100 Microscope).

2.4. *Microhardness and tribological testing*

The indentation tests (0.25 N for 10 s in air at room temperature) were performed on the polished surface of the specimens by loading with a Vickers indenter (Shimadzu HMV 2000). The calculated microhardness values are the average of five measurements. The friction and wear experiments were performed using a pin-on-disc reciprocating flat geometry. A 100C6 steel ball and an alumina ball 6 mm in diameter were used against flat DWCNT/Cu sample surfaces. The sliding speed was fixed at 2 cm s^{-1}. The testing length for one cycle is about 6 mm and a total of 500 cycles were performed for one test. For both steel and alumina balls, the tests were performed at 1 and 5 N. No higher load was tested in order to limit the pellets damage and to avoid changing the contact geometry. The frictional force transferred to a load cell was recorded throughout the test.

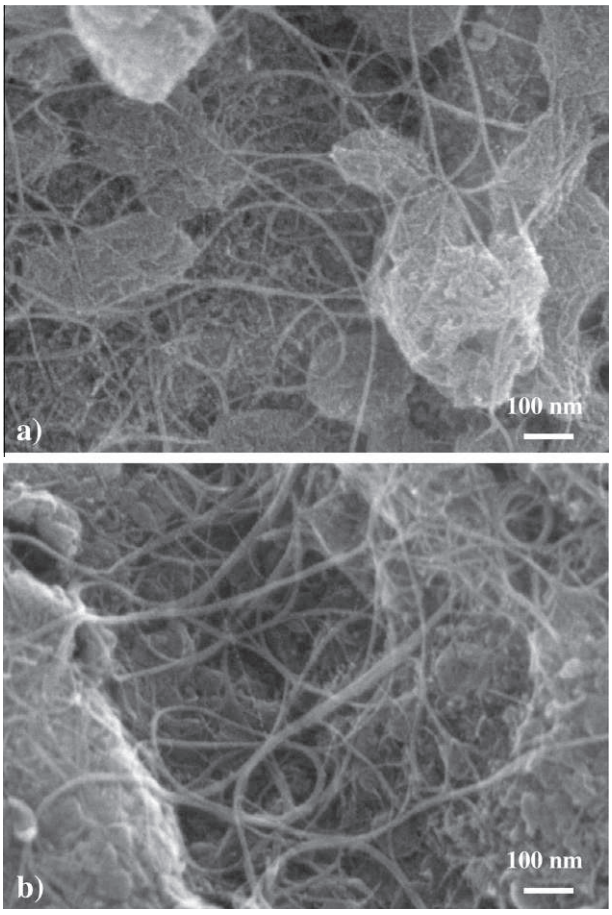

Fig. 3 – Higher-magnification FESEM images of powders P4 (a) and P16 (b).

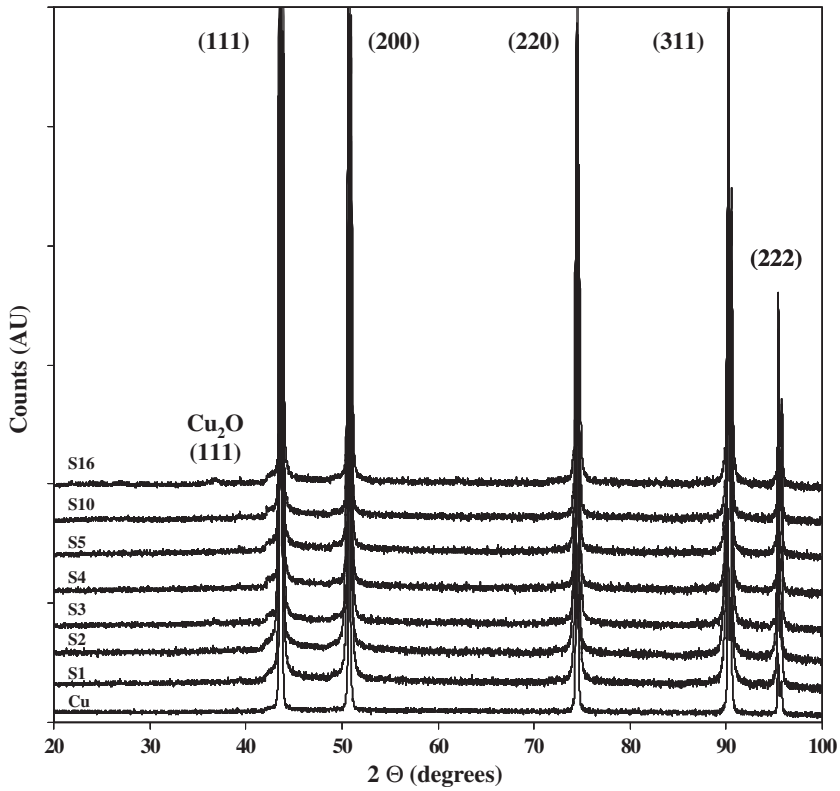

Fig. 4 – XRD patterns of the sintered specimens. Note that the pattern is zoomed and only the bottom fourth of the full Cu (1 1 1) peak is shown.

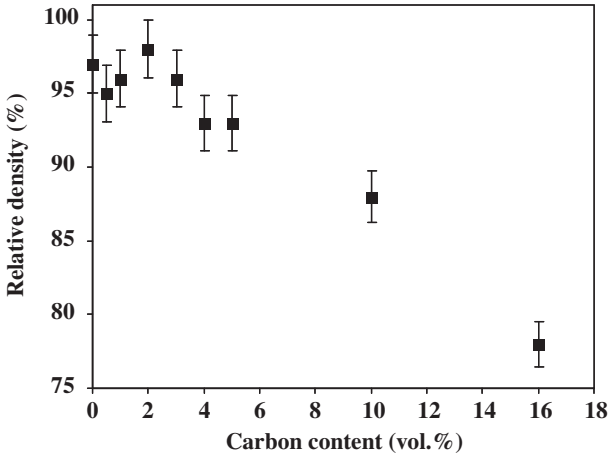

Fig. 5 – Relative density of the specimens prepared by SPS versus the carbon content.

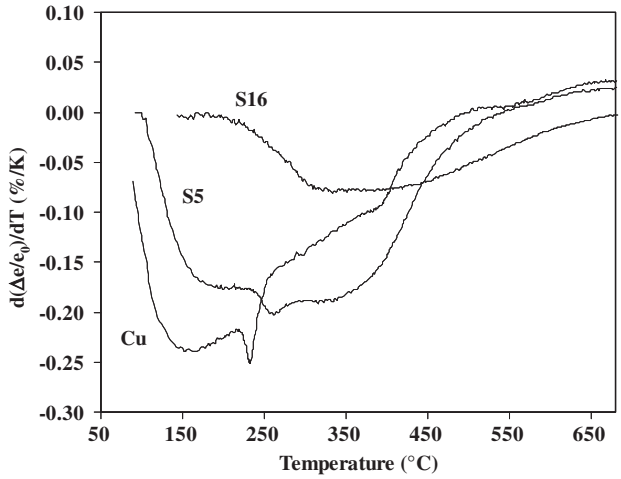

Fig. 6 – The derivative shrinkage curves for pure Cu, S5 and S16.

3. Results and discussion

3.1. *Powders*

Analysis of the XRD patterns (not shown) of the oxide and metal powders shows only the desired compounds, CuO and Cu, respectively. Only the Cu peaks are detected for the composite powders, even for P10 and P16, which could indicate that the CNTs do not form large agglomerates. The specific surface area of the Cu powder is equal to 1.9 m^2/g. The specific surface area of the composite powders (Fig. 1) sharply increases up to 12.7 m^2/g upon the increase in carbon content up to 5 vol%.

This could reflect the increase in the content of DWCNTs, because CNTs contribute much to the specific surface area of a composite powder [21]. However, for higher carbon contents (10 and 16 vol%), the further increase in specific surface area is smaller, which could reflect the higher degree of bundling of the DWCNTs. This could be

due to more bundling in the suspension prior the introduction of the Cu powder and/or to DWCNTs agglomeration due to capillary forces during the freeze-drying step. A typical FESEM image of the Cu powder (Fig. 2a) reveals agglomerates of dendritical copper, tens of micrometers in size. For the P2 powder, there are areas without any observed CNT (Fig. 2b) whereas CNTs are observed in some other areas (Fig. 2c), which could indicate some inhomogeneities of the CNT distribution in the composite powder. Upon increasing the carbon content, more and more CNT-containing areas are observed (Fig. 2d–f).

The CNTs form bundles, their length extending over tens or even hundreds of micrometers. Higher magnification images (Fig. 3) reveal that the bundle diameter tends to increase with the carbon content but is not larger than 40 nm. These observations could reveal that the very short times involved in the sonication and dispersion process, together with freeze-drying, are efficient in preventing both the damaging of the CNTs and the segregation of the low-density CNTs from the much more dense Cu grains.

3.2. *Sintering and microstructure*

Analysis of the XRD patterns (Fig. 4) of the sintered specimens shows only the peaks of Cu. For some specimens, the (1 1 1) peak of Cu_2O carbon is faintly detected, but this could correspond to the oxidation of some grains during the polishing steps. The relative densities are in the range 95–98% for Cu and the S0.5–S3 specimens and decreases regularly for higher carbon contents, as was already observed by other authors [2,4,22,23], reaching only 78% for S16 (Fig. 5).

The shrinkage curves during the ramp up to 700 °C (not shown), i.e. without applied pressure, are similar for all samples except S16. The corresponding derivative curves (Fig. 6) are shown only for selected specimens (Cu, S5 and S16), for the sake of clarity. The first shrinkage step, corresponding to the rearrangement of the copper grains, is at about 100–150 °C for Cu and is shifted to slightly higher temperatures for S5. A second shrinkage step, corresponding to solid-state sintering, is revealed by a sharper peak (at about 230 °C for Cu and 260 °C for S5). For higher temperatures, the dilatation of the graphite stack compensates the shrinkage and becomes predominant above ca. 550 °C, the derivature values becoming positive. By contrast, for S16, the features of the derivative shrinkage curve are less marked and are shifted

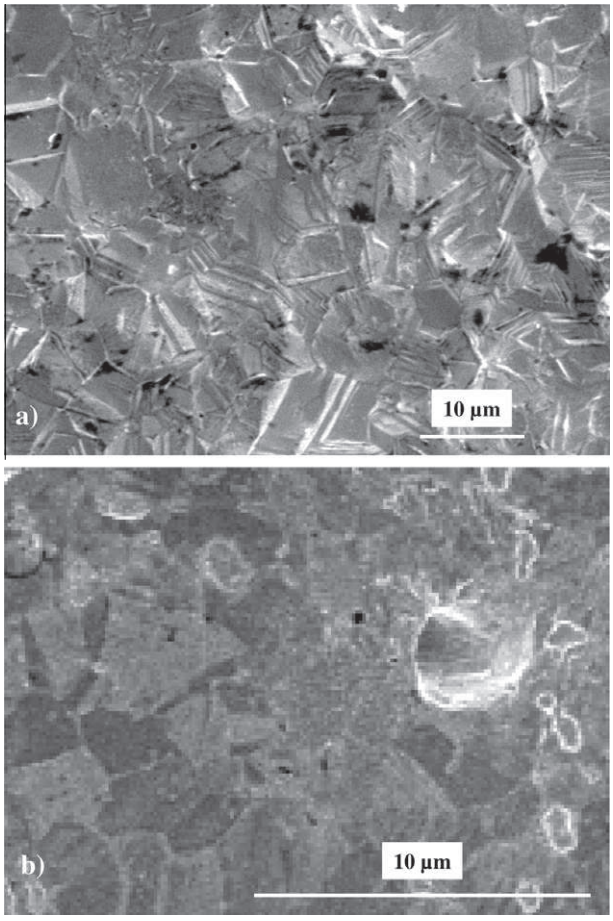

Fig. 7 – FESEM images of the polished and etched surface of the pure Cu specimen (a) and S5 (b).

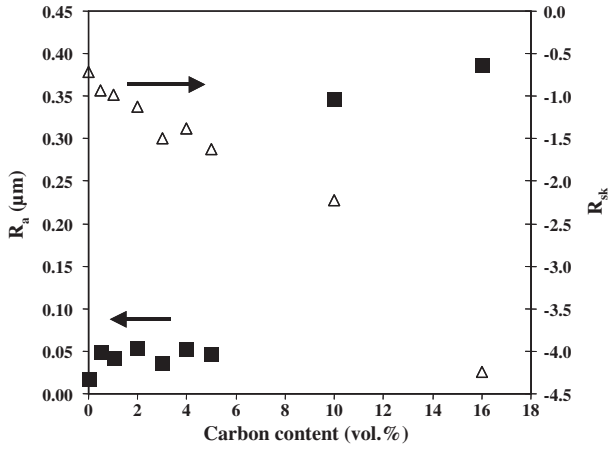

Fig. 8 – Calculated roughness (R_a) (a) and calculated skewness (R_{sk}) versus the carbon content (b). See text for details.

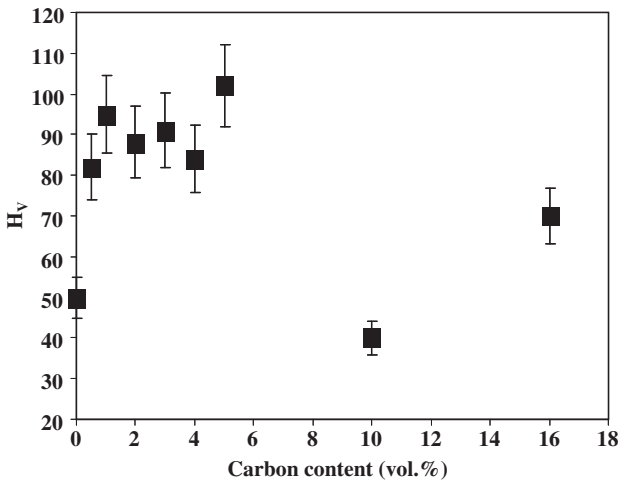

Fig. 9 – Vickers microhardness versus carbon content.

Table 1 – Microhardness and average friction coefficient for different CNT–metal composites. Microhardness tests: Vickers method unless specified: HRB: Rockwell B; HB: Brinell, S: sclerometer.

Ref.	Matrix	Type of CNT	Carbon content	Microhardness	Friction test conditions	Average friction coefficient
This work	Cu	–	–	50	Pin-on-disc, steel/alumina, 5 N	0.80/0.33
	Cu	DWCNT	5 vol%	103		0.25/0.07
[2]	Cu	–	–	98	Block-on-ring, steel, 100 N	0.39
	Cu	MWCNT	15 vol%	116		0.30
	Cu	MWCNT	20 vol%	108		0.29
[3,4]	Cu	–	–	102 (HRB)	Pin-on-disc, diamond, 10 N/30 N	0.27/0.21
	Cu	MWCNT	16 vol%	198 (HRB)		0.13/0.10
[5]	Cu	–	–	58	–	–
	Cu	MWCNT	10 vol%	42	–	–
	Cu (nano)	–	–	74	–	–
	Cu (nano)	MWCNT	10 vol%	102	–	–
[8]	Cu	–	–	118 (S)	–	–
	Cu	SWCNT	7 vol%	143 (S)	–	–
	Cu	SWCNT	10 vol%	161 (S)	–	–
[9]	Al–Mg	–	–	106 (HB)	Pin-on-disc, steel, 30 N	0.147
	Al–Mg	MWCNT	5 vol%	116 (HB)		0.145
	Al–Mg	MWCNT	15 vol%	173 (HB)		0.106
[10]	Al	–	–	44	Pin-on-disc, steel, 2.94 N	0.65
	Al	MWCNT	1 wt%	55		0.61
	Al	MWCNT	5 wt%	54.5		0.68
[11]	Al–Si	–	–	–	Nanoscratch, Berkovich tip, 3 mN	0.18
	Al–Si	MWCNT	5 wt%	–		0.18
	Al–Si	MWCNT	10 wt%	–		0.18
[12]	Ni	–	–	562	Ball-on-plate, steel, 10 N/30 N	–
	Ni	MWCNT	5 vol%	–		1.2/1.0
	Ni	MWCNT	12 vol%	865		0.95/0.75

to higher temperatures. This could reflect firstly that the web-like structure of the DWCNTs becomes very well interconnected, very rigid, and thus inhibits the matrix grains rearrangement process, as was evidenced for CNT–ceramic composites [24], and secondly that a higher CNT content inhibits Cu diffusion and grain growth at higher sintering temperature, in agreement with Kwon et al. [22].

FESEM observations of the polished surfaces (after etching in HCl aqueous solution) of selected specimens appear to reveal Cu grains about 10 μm in size for the pure Cu specimen (Fig. 7a) and 2–3 μm in size for S5 (Fig. 7b), which could reflect that the DWCNTs inhibit the Cu grain growth. This effect was also observed for single-wall CNT/Cu coatings [8].

Interferential rugosimetry allowded one to calculate the average roughness (R_a – Fig. 8) of the surface of the specimens from the data provided by white-light interferometry optical micrographs. For the Cu specimen, R_a is very low (ca. 0.02 μm). It is slightly higher (R_a = 0.05 μm) for S0.5–S5 and markedly higher for S10 and S16 (Fig. 8), which could reflect the lower relative density for the latter specimens. The skewness (R_{sk}), or asymmetry coefficient, was also calculated from the optical micrographs. An R_{sk} value equal or close to zero reflects a gaussian distribution of the topographical heights of a specimen surface. A negative value indicates that topographical profile is mainly made up of valleys, as opposed to peaks. Here, R_{sk} is regularly decreasing upon the increase in carbon content (Fig. 8), from −0.7 for pure Cu to −4.2 for S16. This could reflect that Cu grains are more easily teared off because of the corresponding decrease in density (Fig. 5) and/or because of the presence of CNTs or CNT bundles at the grain boundaries.

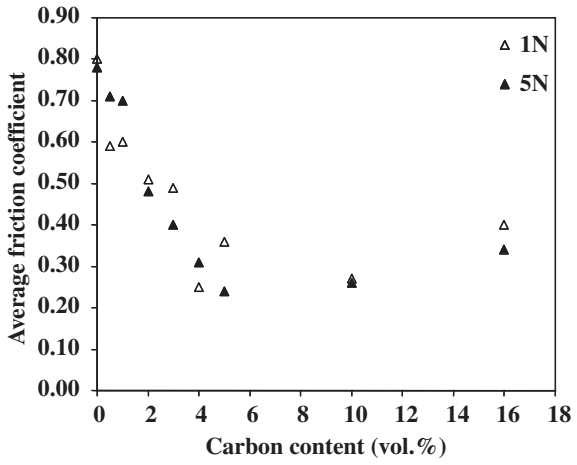

Fig. 10 – Average friction coefficient against a steel ball versus carbon content. The test load is indicated.

3.3. *Microhardness and tribological properties*

The Vickers microhardness for the Cu specimen is equal to 50. The Vickers microhardness is significantly higher for the S0.5–S5 samples (in the range 82–103) and is lower for S10 and S16 (Fig. 9). The increase in microhardness is similar or higher to what has been reported for other CNT/metal composites (Table 1) and is achieved for a lower carbon loading. It could be due to a refinement of the Cu–matrix grain size and to effective load transfer from the matrix to the DWCNTs during the deformation [8], reflecting the high interfacial strength and the homogeneous dispersion of the CNTs within the matrix [6].

The average friction coefficient against a steel ball (Fig. 10) decreases regularly for both applied loads, from about 0.80 (pure Cu, 1 N) to 0.25 (S4, 1 N) and from about 0.78 (pure Cu, 5 N) to 0.24(S5, 5 N). The value remains low for S10 and is slightly higher for S16. The amplitude of the decrease is much higher than was reported for other CNT/metal composites (Table 1).

Typical curves showing the friction coefficient against the steel ball versus the number of cycles are shown in Fig. 11. The behavior at 1 and 5 N is similar, showing a less steeper increase of the friction coefficient and a lower noise once it is stabilized, for the composites than for pure Cu. The observed noise reflects that the contact lacks stability and a certain amount of wear. Nevertheless, wear in general seems limited and a preliminary analysis of the worn surfaces on the specimen and on the steel ball found Cu and carbon debris on the ball.

The average friction coefficient against an alumina ball versus the carbon content is reported in Fig. 12. For an applied load of 1 N, the average friction coefficient decreases from about 0.30 for pure Cu to 0.08 for S5 and then increases,

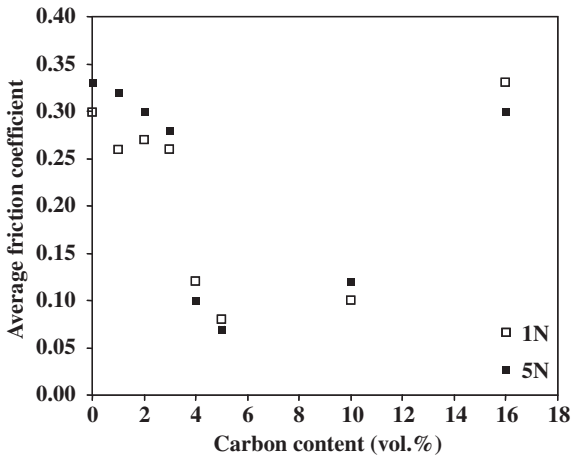

Fig. 12 – Average friction coefficient against an alumina ball versus carbon content. The test load is indicated.

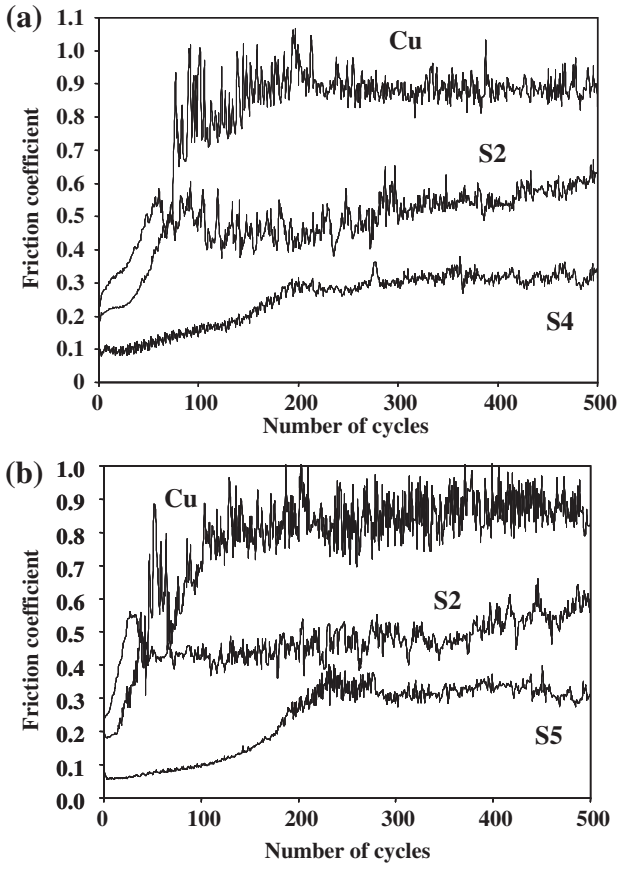

Fig. 11 – Friction coefficient against a steel ball versus the number of cycles for selected specimens. The test load is equal to 1 N (a) and 5 N (b).

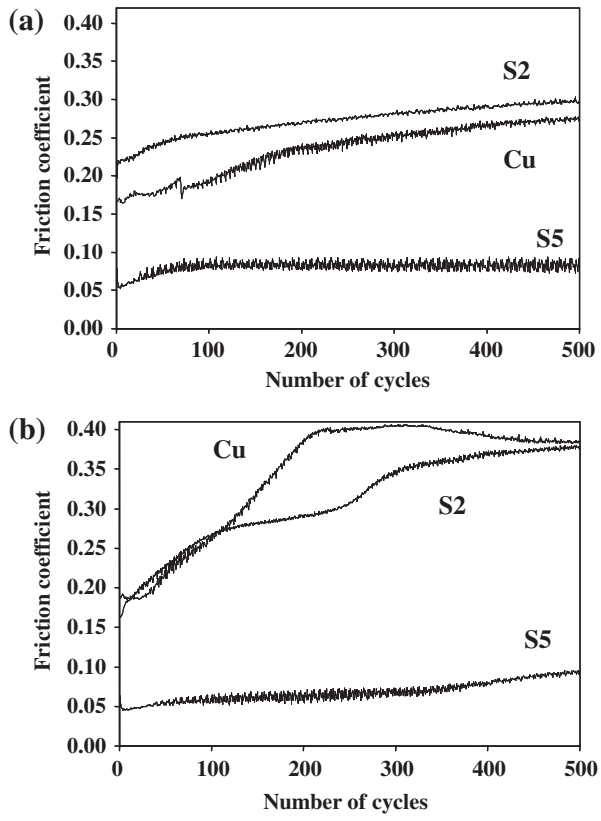

Fig. 13 – Friction coefficient against an alumina ball versus the number of cycles for selected specimens. The test load is equal to 1 N (a) and 5 N (b).

Table 2 – Average and maximum Hertzian contact pressures (P_{Hertz} and P_{max}, respectively) calculated according to Eqs. (1) and (2) (see text for details) using the following values for the Young modulus (E) and Poisson coefficient (ν) of the counterparts: E_{Cu} = 100 GPa, ν_{Cu} = 0.33, E_{steel} = 200 GPa, ν_{steel} = 0.33, $E_{alumina}$ = 390 GPa, $\nu_{alumina}$ = 0.27.

Ball	Load (N)	P_{Hertz} (MPa)	P_{max} (MPa)
Steel	1	330	495
Steel	5	565	850
Alumina	1	370	555
Alumina	5	630	950

reaching 0.35 for S16. For an applied load of 5 N, it decreases markedly from about 0.33 for pure Cu to 0.07 for S5 and then increases, reaching 0.30 for S16. Again, the amplitude of the decrease is much higher than reported before (Table 1).

Curves showing the friction coefficient against an alumina ball versus the number of cycles for selected specimens are shown in Fig. 13. The noise is much lower than against a steel ball (Fig. 11), indicating a much more stable contact and extremely low wear, in agreement with preliminary observations. The minimum friction coefficient reported for the present DWCNT/Cu composites are obtained for a carbon content significantly lower (5 vol%) than contents reported for MWCNT/Cu composites (10–20 vol%) because, as mentioned above, much more DWCNTs are present for a certain carbon loading.

The average and maximum Hertzian contact pressures (P_{Hertz} and P_{max}, respectively) were calculated (Table 2) from the ball-radius (R), the applied load (F), the Young modulus (E) and Poisson coefficient (ν) of the counterparts, using Eqs. (1) and (2):

$$P_{Hertz} = F/\pi a^2 \quad (1)$$

$$P_{max} = 3F/2\pi a^2 \quad (2)$$

where

$$\text{the contact radius } a = (3FR^*/2E^*)^{1/3} \quad (3)$$

the equivalent contact radius R* and the equivalent Young modulus are defined as follows:

$$R^* = R/2 \text{ (ball–plane contact)} \quad (4)$$

$$1/E^* = \left(1 - \nu_{ball}^2\right)/E_{ball} + \left(1 - \nu_{plane}^2\right)/E_{plane} \quad (5)$$

Caillier et al. [25] have calculated the transition pressures for pressure-induced mechanical transitions expected for DWCNTs with an outer diameter of 4 nm. The first transition (ovalization), corresponding to a modification of the outer wall cross-section from circular to oval, could occur above 80 MPa. The second one (collapse), corresponding to the deformation of the outer wall into a peanut-like cross-section, could occur above 540 MPa. These authors [25] note that for DWCNTs, on the one hand, these transitions should take place to higher pressures due to an additional mechanical support by the inner tube, but that on the other hand, the interaction with a substrate (here the matrix surface) should lead to a reduction of the ovalization onset. Li et al. [26] have reported that the average tensile strength of well-aligned DWCNT strands with diameters of 3–20 μm, i.e. similar to the present bundles, is equal to 1.2 GPa. An approximate value of the shear elastic limit would be half that value, i.e. 600 MPa. Bichoutskaia et al. [27] have calculated that 215 MPa is a pressure high enough to relatively shear the CNT walls of individual DWCNTs. Comparing the maximum Hertzian contact pressures (P_{max}) with the data reported by these authors [25–27] could indicate that the friction tests allow for the deformation and breaking of the surface DWCNTs and bundles of them, possibly resulting in the formation of a graphitized lubricating tribofilm in the contact. This could explain the low friction coefficients obtained with both steel and alumina ball counterfaces. The extent and the homogeneity of the DWCNT dispersion is very high and the DWCNTs are very effective in preventing wear by mechanisms involving the plastic deformation of the metal [3,4,12] and the tearing of Cu grains [6]. A uniform distribution of the CNTs was reported to be very important for enhancing the wear resistance of CNT–Al_2O_3 composites [28]. However, a detailed study of wear falls outside the scope of this work and warrants further studies.

4. Conclusions

A marked decrease (by a factor of ca. 4) of the average friction coefficient against a steel ball or an alumina ball is reported for Cu–matrix composites reinforced with DWCNTs, compared to pure copper. The deformation and breaking of the surface DWCNTs and bundles of them during the friction tests could result in the formation of a graphitized lubricating tribofilm in the contact, as revealed by maximum Hertzian contact pressure data. The presence of the DWCNTs also provokes a doubling of the Vickers microhardness. These results arise because of the unique microstructure in terms of DWCNTs length and quality, DWCNT content and matrix grain size, achieved through the use of a rapid route involving freeze-drying, without oxidative acidic treatment or ball-milling, for the synthesis of composite powders and through consolidation by SPS. The best results are obtained for a carbon loading (5 vol%) significantly lower than those reported when using MWCNTs (10–20 vol%), because there are much more CNTs, and the extent and homogeneity of their dispersion is better, when using DWCNTs as opposed to MWCNTs.

Acknowledgments

The authors thank L. Datas for assistance in the FESEM observations, which were performed at TEMSCAN, the “Service Commun de Microscopie Electronique à Transmission”, Université Paul-Sabatier (Toulouse). The authors also thank G. Chevallier for assistance with the SPS, which was performed at the Plateforme Nationale CNRS de Frittage Flash (PNF^2, Toulouse) and V. Baylac for assistance with the rugosimetry. This work is performed within the framework of the Fédération de Recherche pour l’Aéronautique et l’Espace program (FRAE AO4).

REFERENCES

[1] Bakshi SR, Lahiri D, Agarwal A. Carbon nanotube reinforced metal–matrix composites – a review. Int Mater Rev 2010;55(1):41–64.

[2] Dong SR, Tu JP, Zhang XB. An investigation of sliding wear behavior of Cu–matrix composite reinforced by carbon nanotubes. Mater Sci Eng A 2001;313(1–2):83–7.
[3] Tu JP, Yang YZ, Wang LY, Ma XC, Zhang XB. Tribological properties of carbon-nanotubes-reinforced copper composites. Tribol Lett 2001;10(4):225–8.
[4] Chen WX, Tu JP, Wang LY, Gan HY, Xu ZD, Zhang XB. Tribological application of carbon nanotubes in a metal-based composite coating and composites. Carbon 2003;41(2):215–22.
[5] Kim KT, Lee KH, Cha SI, Mo CB, Hong SH. Characterization of carbon nanotubes/Cu nanocomposites processed by using nano-sized Cu powders. Mater Soc Symp Proc 2004;821:P3.25.1–6.
[6] Kim KT, Cha SI, Hong SH. Hardness and wear resistance of carbon nanotube reinforced Cu–matrix nanocomposites. Mater Sci Eng A 2007;449–451:46–50.
[7] Cha SI, Kim KT, Arshad SN, Mo BC, Hong SH. Extraordinary strengthening effect of carbon nanotubes in metal–matrix nanocomposites processed by molecular-level mixing. Adv Mater 2005;17(11):1377–81.
[8] Yang YL, Wang YD, Ren Y, He CS, Deng JN, Nan J, et al. Single-walled carbon nanotube-reinforced copper composite coatings prepared by electrodeposition under ultrasonic field. Mater Lett 2008;62(1):47–50.
[9] Zhou SM, Zhang XB, Ding ZP, Min CY, Xu GL, Zhu WM. Fabrication and tribological properties of carbon nanotubes reinforced Al composites prepared by pressureless infiltration technique. Composites Part A 2007;38(2):301–6.
[10] Kim IY, Lee JH, Lee GS, Baik SH, Kim YJ, Lee YZ. Friction and wear characteristics on the carbon nanotube–aluminum composites with different manufacturing conditions. Wear 2009;267(1–4):593–8.
[11] Bakshi SR, Lahiri D, Patel RR, Agarwal A. Nanoscratch behavior of carbon nanotube reinforced aluminum coatings. Thin Solid Films 2010;518(6):1703–11.
[12] Chen XH, Chen CS, Xiao HN, Liu HB, Zhou LP, Li SL, et al. Dry friction and wear characteristics of nickel/carbon nanotubes electroless composite deposits. Tribol Int 2006;39(1):22–8.
[13] Monthioux M, Smith BW, Burteaux B, Claye A, Fischer JE, Luzzi DE. Sensitivity of single-wall carbon nanotubes to chemical processing: an electron microscopy investigation. Carbon 2001;39(8):1251–72.
[14] Zhang SC, Fahrenholtz WG, Hilmas GE, Yadlowski EJ. Pressureless sintering of carbon nanotube–Al_2O_3 composite. J Eur Ceram Soc 2010;30(6):1373–80.
[15] Laurent Ch, Flahaut E, Peigney A. The weight and densities of carbon nanotubes versus the number of walls and diameter. Carbon 2010;48(10):2989–99.
[16] Legorreta Garcia F, Estournès C, Peigney A, Weibel A, Flahaut E, Laurent Ch. Carbon nanotube–magnesia nanocomposites by spark-plasma-sintering: microstructure, electrical conductivity and microhardness. Scr Mater 2009;60(9):741–4.
[17] de Andrade MJ, Weibel A, Laurent Ch, Roth S, Pérez Bergmann C, Estournès C, et al. Electrical conductive double-walled carbon nanotubes–silica glass nanocomposites prepared by the sol–gel process and spark plasma sintering. Scr Mater 2009;61(10):988–91.
[18] Peigney A, Legorreta Garcia F, Estournès C, Weibel A, Laurent Ch. Toughening and hardening in double-walled carbon nanotube/nanostructured magnesia composites. Carbon 2010;48(7):1952–60.
[19] Flahaut E, Bacsa R, Peigney A, Laurent Ch. Gram-scale CCVD synthesis of double-walled carbon nanotubes. Chem Commun 2003:1442–3.
[20] Flahaut E, Peigney A, Laurent Ch, Rousset A. Synthesis of single-walled carbon nanotube–Co–MgO composite powders and extraction of the nanotubes. J Mater Chem 2000;10(2):249–52.
[21] Peigney A, Laurent Ch, Dobigeon F, Rousset A. Carbon nanotubes grown in-situ by a novel catalytic method. J Mater Res 1997;12(3):613–5.
[22] Kwon Y-S, Chung S-T, Lee S, Noh J-W, Park J-S, German RM. Development of carbon nanotube reinforced copper. Adv Powder Metall 2008;9:296–305.
[23] Daoush WM. Processing and characterization of CNT/Cu nanocomposites by powder technology. Powder Metall Met Ceram 2008;47:9–10.
[24] Peigney A, Rul S, Lefèvre-Schlick F, Laurent Ch. Densification during hot-pressing of carbon nanotube–metal–ceramic composites. J Eur Ceram Soc 2007;27(5):2183–93.
[25] Caillier Ch, Ayari A, Gouttenoire V, Benoit JM, Jourdain V, Picher M, et al. An individual carbon nanotube transistor tuned by high pressure. Adv Funct Mater 2010;20(19):3330–5.
[26] Li Y, Wang K, Wei J, Gu Z, Wang Z, Luo J, et al. Tensile properties of long aligned double-walled carbon nanotube strands. Carbon 2005;43(1):31–5.
[27] Bichoutskaia E, Ershova OV, Lozovik YE, Popov AM. Ab initio calculations of the walls shear strength of carbon nanotubes. Tech Phys Lett 2009;35(7):666–9.
[28] Lim DS, You DH, Choi HJ, Lim SH, Jang H. Effect of CNT distribution on tribological behavior of alumina–CNT composites. Wear 2005;259(1–6):539–44.